SLAC – PUB – 4128
March 1988
T/E

Electroweak Cross Sections and Asymmetries at the Z° *

D. C. KENNEDY, B. W. LYNN, C. J.–C. IM

Institute for Theoretical Physics, Department of Physics

and

Stanford Linear Accelerator Center
Stanford University, Stanford, California 94309

and

R. G. STUART

Max-Planck-Institut für Physik und Astrophysik
München, Federal Republic of Germany

ABSTRACT

We present complete calculations for basic observables at the SLC/LEP e^+e^- colliders: the Z° cross sections, line shape and width, forward-backward and polarization asymmetries. The effects of experimental cuts are explored. Special emphasis is placed on the polarization asymmetry, a highly sensitive measure of electroweak couplings and of the presence of heavy particles in virtual loops. The calculations were performed using a new, more efficient Monte Carlo method, which is also discussed.

Submitted to *Nuclear Physics B*

---

*Work supported by the Department of Energy, contract DE–AC03–76SF00515 and the National Science Foundation, contract NSF–PHY–86–12280.

1. Introduction: Physics at the Z° Peak

The imminent arrival of the SLC and LEP electron-positron colliders promises extensive and detailed tests of the standard Glashow–Salam–Weinberg model of electroweak physics. Both of these accelerators will carry out their first experiments at the Z° resonance and will probe the electroweak neutral current with great precision, requiring correspondingly accurate theoretical predictions based on the standard model. Although a wide variety of measurements will be performed at these machines, we study in this paper the physical properties and computation of an important subset of measurements, the inclusive or semi-inclusive quantities arising from the decay of the Z° in the s channel into charged fermion-antifermion pairs (excluding electron-positron pairs; i.e., Bhabba scattering): total cross sections; the Z° peak position, width and line shape; and the forward-backward and left-right polarization asymmetries. We will examine the result of experimental cuts and, where relevant, the polarization of the electron beam. The polarization asymmetry is of special importance, as it is not sensitive to "difficult" physics, such as the hadronization of final-state quarks, but exquisitely sensitive to particles appearing in virtual loops. The results presented here are accurate predictions for these quantities based on calculations as complete as necessary, up to the theoretical uncertainties discussed below.

All of the above quantities are derived from cross section measurements. The forward-backward asymmetry is:

$$A_{FB} = \frac{\sigma_F - \sigma_B}{\sigma_F + \sigma_B} \quad , \tag{1.1}$$

where F and B are the *fermion* cross sections in the forward and backward hemispheres, respectively, of the experimental detector. The polarization asymmetry is defined as:

$$A_{LR} = \frac{\sigma_L - \sigma_R}{\sigma_L + \sigma_R} \quad , \tag{1.2}$$

where L and R refer to the left and right longitudinal polarization states of the incoming electron. We can also define a *polarized* forward-backward asymmetry:[1]

$$A_{FB}^{pol} = \frac{(\sigma_{LF} - \sigma_{RF}) - (\sigma_{LB} - \sigma_{RB})}{(\sigma_{LF} + \sigma_{RF}) + (\sigma_{LB} + \sigma_{RB})} \quad . \tag{1.3}$$

The Z° line shape itself refers to the measured cross section. All of these quantities can be defined for various species of final-state fermions and also inclusively, after summing over all observed species. Precise theoretical predictions of these measurables require radiative corrections to the tree-level graphs. These fall into a number of classes (Fig. 1):[2,3,4] the "oblique" loop (or gauge boson self-energy) corrections (Fig. 1a); the "direct" loop corrections, vertices (Fig. 1b) and boxes (Fig. 1c); and the bremsstrahlung, or radiation, graphs (Fig. 1d). The direct corrections can be further divided into subclasses: *QED* graphs, vertices and boxes involving at least one photon, and *weak* graphs, vertices and boxes containing only massive weak gauge bosons. The vertices can occur in either the initial or final state. The QED graphs must be treated separately because they contain infrared divergences. Each direct QED graph must be combined with the corresponding bremsstrahlung graphs to obtain a finite result. Hence, we can refer collectively to the "initial," "final" and "initial/final" QED corrections. In Table I we show the generic magnitude of these corrections to the various observables at the Z° peak. By far the most important correction to the cross section and A_{FB} comes from the initial-state QED radiation, which distorts the shape of Z° resonance. Furthermore, to reach the necessary accuracy in the cross sections, one needs to include higher-order radiation emission from the initial state up to at least two photons.[5] This is best done by the procedure of "exponentiation," which includes the effect of an infinite number of photons.[6,7] (Most of the initial radiation is soft.) On the other hand, A_{LR} is most sensitive to the oblique and initial weak corrections. Keeping in mind the limits on the experimental measurement of these quantities (listed in Table I), we see that the three sets of corrections, *initial QED (vertex and radiation), oblique* and *initial weak,* are all that are necessary to make adequate predictions for the observables in question.

Our approach will therefore be to construct simple expressions for the cross sections that contain only these corrections. We explain this simple ansatz and a new Monte Carlo technique developed to apply it in Section 2. In Sections 3 and 4 we present the results of this Monte Carlo for our set of observables: cross sections, properties of the Z° line shape and asymmetries. We also discuss some of the effects of residual corrections not included in this Monte Carlo. In addition to numerical predictions, we discuss in some detail the effects of polarization, experimental cuts and virtual particles on the radiative corrections.

2. EXPOSTAR: Physical Ansatz and Monte Carlo Method

A simple Monte Carlo with the necessary corrections, EXPOSTAR, has been developed. As discussed below, we have also used another program, BREM5, a complete order α Monte Carlo based on the Berends–Kleiss generator, to check some of the results obtained with EXPOSTAR.[8]

To construct the ansatz, we begin with the tree-level neutral-current amplitude, written schematically without tensor or spinor indices as:[2]

$$M_{NC} = \frac{e^2 QQ'}{q^2} + \frac{e^2 (I_3 - s_\theta^2 Q)(I'_3 - s_\theta^2 Q')/s_\theta^2 c_\theta^2}{q^2 + \frac{e^2}{4\sqrt{2} s_\theta^2 c_\theta^2 G_\mu \rho} + i\sqrt{s}\,\Gamma_Z} \quad ; \tag{2.1a}$$

$$\frac{\Gamma_Z}{\sqrt{s}} = \frac{e^2}{12\pi s_\theta^2 c_\theta^2} \sum_f \left[\left(\frac{I_{3f}}{2} - Q_f s_\theta^2 \right)^2 \left(1 - \frac{2m_f^2}{q^2} \right) + \left(\frac{I_{3f}}{2} \right)^2 \left(1 + \frac{4m_f^2}{q^2} \right) \right] \cdot \sqrt{1 + \frac{4m_f^2}{q^2}} \cdot C_{QCD} \quad ; \tag{2.1b}$$

$$C_{QCD} = 1 \text{ for leptons} \quad ,$$

$$= 3 \cdot \left(1 + \frac{\alpha_s(q^2)}{\pi} \right) \text{for quarks} \quad ; \quad s = -q^2 \quad ,$$

where "f" stands for sum over all accessible (low mass) fermions. In the s (annihilation) channel, $q^2 = -s$. The gauge-fermion couplings have been written in terms of the *fermion* quantum numbers, unprimed for initial state, primed for final. Q is the electric charge (in proton units) and I_3 is the weak (left-handed) isospin. The amplitude has been written to make the different electroweak parameters evident: the electroweak mixing s_θ^2, $c_\theta^2 = 1 - s_\theta^2$, e^2, the Fermi constant G_μ and ρ. The oblique corrections can be completely and self-consistently subsumed in one stroke by converting each of these fixed parameters to the corresponding universal "starred" function that runs with q^2:

$$s_*^2(q^2), c_*^2(q^2), e_*^2(q^2), G_{\mu_*}(q^2), \rho_*(q^2) \quad . \tag{2.2}$$

The definition, properties and explicit one-loop computation of the starred functions were discussed extensively in a previous paper.[9] Precise predictions for the four basic starred functions are shown in Fig. 2. The gauge boson self-energies contain hadronic contributions computed via dispersion relations where necessary.[10] The starred functions are defined by a standard set of electroweak parameters (α_{em}, G_μ, M_Z) and knowledge of the radiative corrections. The next step is to include the weak vertex corrections. This can be done by modifying the tree-level gauge-fermion couplings. The electric charge (the fermion-photon coupling) is modified for left- and right-handed particles:[3,9,11]

$$\begin{aligned} Q_L &= Q[1 + V_L(q^2)] + I_3 V_L{}^{nAb}(q^2) \quad ; \\ Q_R &= Q[1 + V_R(q^2)] \quad . \end{aligned} \tag{2.3}$$

The fermion-Z coupling is modified for left- and right-handed particles:

$$\begin{aligned} g_L &= (I_3 - s_*{}^2(q^2)Q)[1 + V_L(q^2)] + c_*{}^2(q^2) I_3 V_L{}^{nAb}(q^2) \quad ; \\ g_R &= (-s_*{}^2(q^2)Q)[1 + V_R(q^2)] \quad . \end{aligned} \tag{2.4}$$

The three V functions are defined in Ref. 9 in terms of the fermion's quantum numbers, Q and I_3, and a pair of virtual loop functions. These latter functions are universal for light fermions, depending only on q^2 and the W and Z masses. Assuming that the final-state fermions are also light, the modified couplings can be used for both initial and final weak vertices.

We now are left with the initial-state QED corrections to consider. There are a number of approaches to the initial-state radiation problem. A standard path, pioneered by Berends and Kleiss,[8] is to consider the emission of one photon, then extend the calculation to two photons (Berends et al.)[5] or, through exponentiation, to an arbitrary number of photons (Ward[7] and Jadach[12]). Another way to calculate the initial state QED is to ignore any explicit consideration of photon dynamics and to regard the radiation as simply changing the energy-momentum spectrum of the e^+e^- beams. This method is perfectly tailored to

the present case, where we are interested only in the final-state fermions and the indirect effects of the photon emission on them, and not in the radiation itself. Analytic calculations of this type have been developed by Cahn[13] and Alexander et al.[14] Following the work of Trentadue and Nicrosini,[15] Kuraev and Fadin,[16] and Altarelli and Martinelli,[17] we can write the initial state QED corrections to the cross section in a "parton-like" representation, by convolving a radiationless "tree-level" cross section $\sigma_0(s)$ with the electron and positron structure functions $D(x,s)$:

$$\sigma(s) = \int dx_+ dx_- D(x_+,s) D(x_-,s) \sigma_0(s') \quad . \tag{2.5}$$

The physical content of this approach is clear. The e^+ beam loses some momentum to radiation, and its energy is reduced to a fraction x_+ of its original value. The e^- beam energy is reduced to x_-. The structure functions describe the spectrum of the electron and positron beams, without explicitly describing the emission of individual photons. The total cross section is then a convolution over all possible ways of losing energy, with the unconvoluted cross section σ_0 evaluated at the reduced s, $s' = x_+ x_- s$, in a new center-of-mass (cm) frame moving collinear to the beams. Of course, the radiation from the initial beams is not entirely collinear, but has a transverse component. The transverse degree of freedom is present in Eq. 2.5, but has been integrated over, so that its presence is implicit in the function $D(x,s)$. The crucial point about the factorized form of Eq. 2.5 is that the integration over the transverse momentum $\vec{p}_\perp$ assumes *no cuts*.[18] The structure functions can be computed to the desired accuracy using evolution equations analogous to the Altarelli–Parisi equations of QCD. In the EXPOSTAR Monte Carlo, we make use of the structure functions of Nicrosini and Trentadue.[15] These form factors contain the large infrared logarithms summed to all orders of α, a special case of "exponentiation." In addition, they contain purely ultraviolet logarithms to order α^2. As such, these form factors include the same contributions to the total cross section as a complete order α^2 calculation would and are thus adequate for our purposes (compare, Section 1).

If angular cuts are made in Eq. 2.5, the neglect of transverse radiation induces an error in the cross section. The same problem occurs in the differential cross section because the differential cross section is, after all, just a special kind of "cut" cross section. Our ansatz, based on Eq. 2.5, is:

$$\frac{d\sigma(s)}{d\Omega_{lab}} = \int dx_+ dx_- D(x_+,s) D(x_-,s) \frac{d\sigma_0(s)}{d\Omega_{cm}} \frac{d\Omega_{cm}}{d\Omega_{lab}} \quad . \tag{2.6}$$

Such an approximation is unacceptable for general applications but is quite sufficient in our case. To order α, both analytic and numerical treatments show that the distribution of transverse momentum from initial-state radiation is contained almost entirely below 1 GeV and is concentrated heavily in the low hundreds of MeV. Such momenta are small enough to be considered as perturbations on the motion determined solely by the longitudinal radiation and effectively give rise to an intrinsic uncertainty in the angles of the final-state fermions. The effect of such uncertainties on the cross sections is small (on the order of a few tenths of a percent) and negligible on the asymmetries. (See Table I.) A direct confirmation is provided by BREM6, which contains the same exponentiated initial QED as EXPOSTAR, but with the one-photon contribution removed and computed instead by the Berends–Kleiss generator of BREM5. These results will be presented in a later paper.[19] The higher-order transverse momentum distribution is still unknown. Since the order α transverse effect is small, however, it seems reasonable to assume that the higher-order distribution of $\vec{p}_\perp$ will have no significant effect on the experimental observables in question. In particular, we expect that any changes in the transverse distribution will occur mainly in the low hundreds of MeV region, while not markedly increasing the number of worrisome events with large $\vec{p}_\perp$. We should note here that EXPOSTAR is *not* designed to provide a realistic simulation of the final–state fermions *on an event-by-event basis,* but is rather a Monte Carlo *integration* routine that computes such integrals as Eq. 2.5. This fact alleviates the limitation of missing the transverse degree of freedom.

Without cuts, the integration in Eq. 2.5 could be carried out analytically, but the presence of cuts makes a Monte Carlo essential. The integrations in

EXPOSTAR are rewritten in terms of an approximant cross section and radiation distribution. One then generates events by sampling in the space of the approximant. This space has some irregular shape, with a sharp, high peak at the Z°. The usual way of sampling such an irregular space is to put a "box" around it large enough to contain the space's widest dimension. Points are then sampled uniformly in the box ("events") and are thrown away ("rejected") if they do not lie within the actual irregular Monte Carlo space. For Z° physics, this approach is very inefficient, because most of the box's volume lies outside the space to be sampled, and the points generated in this region will be rejected. This problem led us to invent a new method, efficient and elegant, that involves no rejection procedure. As described in the Appendix and in another paper,[20] the actual integrand Eq. 2.5 is discretized so that its volume can be easily evaluated as the sum of individual cells ("noodles") and sampled efficiently without rejection. The sampling space can be carved up into "noodles" in any fashion whatsoever, the better to handle any particular peaking structure at hand. This turns out to be especially crucial at energies above the Z°, as the resonance peak becomes very narrow in the approximant space. A conventional rejection-based Monte Carlo would encounter grave difficulties here, as the number of events would have to increase rapidly in order to sample the peak properly.

With the electroweak parameters adjustable by hand, results from EXPOSTAR reproduce two earlier calculations of the cross section[5] and left-right asymmetry,[13] respectively, as shown in Figs. 3 and 4. For the final EXPOSTAR, the tree-level cross section σ_0 was "decorated" by changing the electroweak parameters to starred functions and modifying the gauge couplings, as outlined above; the electroweak parameters are then not arbitrarily adjustable, but computed self-consistently on the basis of the standard model. For purposes of comparison, we show in Fig. 5 the forward-backward and left-right asymmetries predicted by EXPOSTAR together with two previous calculations, that of Lynn and Stuart[21] (containing no initial-state radiation) and the prediction of BREM5 (which contains just one initial photon). All three calculations contain

the oblique and weak vertex corrections. In keeping with the general properties of the radiation, the lowest-order bremsstrahlung prediction *overestimates* the initial-state QED correction to both A_{FB} and A_{LR} (as do the results of Jadach et al.).[22] BREM5 also allows the addition of the weak box, initial/final and final QED corrections, effects touched on below with regard to A_{LR}.

3. Z° Physics: Cross Sections and Widths

In this section we present some typical results for the Z° peak cross section and line shape, including the effect of cuts and virtual corrections, postponing discussion of the asymmetries to the next section. Following Table I, we note that the effects missing in EXPOSTAR limit the accuracy of the cross section calculation to approximately 1.5%. There is also the statistical error inherent in the Monte Carlo method; all of the results were run with 10^5 events, limiting the statistical error to approximately 0.3%.

We use a canonical parameter set: $M_Z = 94$ GeV, $m_{\text{Higgs}} = 100$ GeV, and $m_{\text{top}} = 60$ GeV, with no detector cuts and a final-state fermion-antifermion energy cut of 10 GeV, which is necessary to avoid the photon pole at $q^2 = 0$. Figure 6a shows the Z° peak as it appears for the muon, hadron and total fermion cross sections (Table II). The Z° width for this case is 2.76 GeV, with a hadronic contribution of 1.94 GeV (including QCD corrections) and a leptonic contribution of 820 MeV. Figure 6b illustrates a blown-up section of the peak for the muon and total cross sections, demonstrating how the peak is shifted from 94 GeV by radiation. (Actually, even the tree-level cross section peak is above 94 GeV, because of the photon exchange.) Note in particular that the peak positions for muon, hadron and total cross sections are indistinguishable. The hadronic cross sections do not contain any final-state QCD corrections.

Detector cuts will be standard in SLC/LEP experiments. A common cut is the *endcap acceptance cut,* which limits the angle of the final-state fermion with respect to the beam axis to some minimum value. For simplicity we use a symmetrical endcap cut. Figure 7 (also Table III) shows the reduction of the muon cross section as we apply more and more restrictive endcap cuts. The peak position suffers no apparent change, however. Another cut often used in experimental analysis is the *acollinearity cut,* which places an upper limit on the acollinearity angle of the final-state antifermion relative to the final-state fermion's axis. (An acollinearity angle of zero means that the fermion-antifermion

pair is emitted back-to-back in the detector frame.) As most of the radiation is soft, the events generally have small acollinearities, so that even a tight cut of 2° reduces the cross section by only a small amount (Table III).

We saw from Table I that the oblique corrections had a small effect on the peak cross section. This result holds even for very large oblique corrections, such as those coming from a large top quark mass. (A large Higgs mass has an analogous but smaller effect.) The general effect of these corrections was discussed in Refs. 2, 9 and 21. Certain gauge parameters are strongly affected by large oblique corrections. This is evident in the Z° width, for example (Table IV). For top quarks as light as 30 GeV, the width contains an open top channel. As the top mass rises, this channel is cut off once the open top threshold reaches 94 GeV, and the width drops. However, the top quark continues to have an indirect effect on the width through virtual loops that renormalize the couplings, and the width rises. (Figure 8 shows how $s^2_*(Z)$ varies with the top quark and Higgs masses.) This effect is of potential importance, as the Z° width will be used to count neutrino generations. Some limit on the top mass is necessary to make sure that the "missing," or "invisible," width of the Z° is correctly attributed to neutrinos and is not due to virtual corrections. Although the width is affected by oblique renormalizations, the peak cross section is almost completely insensitive to them. At the pole, the gauge couplings in the width (Eq. 2.1b) exactly cancel the gauge couplings in the numerator of the matrix element (Eq. 2.1a), so that even a large top mass has a negligible effect. This cancellation is crucially based on a self-consistent treatment of the oblique corrections throughout the matrix element.[9] Self-inconsistencies will lead to faulty results, as illustrated in the recent papers of Berends et al.[23] and Hollik.[24] (Both papers report large peak cross section shifts from a heavy top quark.) In any case, this cancellation limits the usefulness of cross section measurements in making sensitive tests of electroweak couplings and virtual corrections. For such precision, we must to turn to the various asymmetries.

4. Z° Physics: Asymmetries

For precision tests of electroweak physics, the various asymmetries discussed earlier have a number of advantages over cross section measurements alone. Being ratios of cross sections, they are not very sensitive to the luminosity errors that limit cross section measurements. Careful choice of polarization states can isolate different electroweak couplings. The forward-backward asymmetry is one direct measure of parity-violating couplings. At tree level, apart from photon channel terms suppressed by $(\Gamma_Z/M_Z)^2$:

$$A_{FB}(Z) \simeq \frac{3}{4}\left(\frac{g_L^2 - g_R^2}{g_L^2 + g_R^2}\right)^e \left(\frac{g_L^2 - g_R^2}{g_L^2 + g_R^2}\right)^f \quad , \tag{4.1}$$

where the g's are the fermion-Z couplings defined in Section 2, and e and f refer to the initial electron and final fermion, respectively. A_{FB} depends on both the initial and final fermion couplings. It has, however, a number of serious limitations. At the Z° pole, A_{FB} is close to zero and is not strongly affected by large oblique corrections, making it a poor measure of the fermion couplings (Table I). The most severe drawback is that A_{FB} can only be cleanly measured for muons and taus, as only these can be unambiguously identified in the final state by the detector. The final-state quarks suffer hadronization and decays, making measurement of their A_{FB} difficult. Measurements of A_{FB} for muons are subject to poor statistics and a large experimental error ($< 3\%$ branching ratio). All of these problems can be overcome by use of another, more powerful, quantity, the left-right polarization asymmetry A_{LR}. At tree level:

$$A_{LR}(Z) \simeq \left(\frac{g_L^2 - g_R^2}{g_L^2 + g_R^2}\right)^e \quad . \tag{4.2}$$

Unlike A_{FB}, A_{LR} depends only on the *initial-state* couplings, up to small denominator terms proportional to $(\Gamma_Z/M_Z)^2$ (not shown). Hence it is *universal* to all final-state fermion species. As shown by Lynn and Verzegnassi,[25] this

result continues to hold even in the presence of final-state photon and gluon bremsstrahlung and hadronization. Thus, all of the final-state fermion data (excluding e^+e^- pairs) can be used to measure A_{LR}, greatly improving the statistics. Moreover, A_{LR} is nearly independent of initial-state radiation (compare, Table I), as the radiation affects the left and right cross sections almost equally.[25,26] It is also independent of other initial-state effects, such as pair production.[27] (This contradicts the results of Jadach et al.)[22] On the other hand, because of its structure, A_{LR} is exquisitely sensitive to anything that changes the initial-state e^+e^- couplings to the Z° and so serves as the ideal test of the standard electroweak model. Some of the same advantages of polarized beams accrue to the polarized forward-backward asymmetry.[1] At tree-level:

$$A_{FB}^{pol}(Z) \simeq \frac{3}{4}\left(\frac{g_L^2 - g_R^2}{g_L^2 + g_R^2}\right)^f \quad , \tag{4.3}$$

so that A_{FB}^{pol} is in some sense the complement of A_{LR}, in that it measures only the final-state couplings. Since it is not universal to all species, it still suffers from poor statistics. However, there is some hope of measuring both the polarized and unpolarized forward-backward asymmetries for the bottom and charm quarks by tagging their decay products.

Unlike the cross section calculations, the asymmetries predictions are not limited by the radiative corrections left out of EXPOSTAR (Table I). The only uncertainties are statistical; with 10^5 events, they are again of the order of a few tenths of a percent. The excellent weight distribution of EXPOSTAR actually brings these Monte Carlo errors down below the usual statistical level of $1/\sqrt{N_{\text{events}}}$.

The results for the asymmetries evaluated at the Z° pole with the canonical parameters are displayed in Table II. Figure 9 shows how the forward-backward asymmetries vary with energy, using the same parameters. A_{FB}^{pol} demonstrates the advantage of polarized beams. Polarization has made the asymmetry larger than A_{FB} at the Z°, essentially independent of beam energy, and thus easier to

measure. Earlier, in Figure 5, we saw how $A_{LR}(Z)$ was almost independent of initial-state radiation. Figure 10 demonstrates the weak dependence of $A_{LR}(Z)$ on final-state species, for muons, up and down quarks, all hadrons and all fermions (also Table II). Independence of the final state also means that A_{LR} is insensitive to cuts (Table V). A_{FB}, on the other hand, does depend on experimental cuts, as shown in Figure 11 and Table III.

The key property of the left-right asymmetry, its sensitivity to oblique corrections, is illustrated in Table IV and Figure 12. (Table IV also shows the inadequacy of A_{FB} in this regard.) The nature of A_{LR} makes it by far the most delicate measure of the electroweak couplings. All oblique corrections will renormalize the function $s^2_*(Z)$ and so affect $A_{LR}(Z)$:

$$\delta A_{LR}(Z) \simeq -8\delta s^2_*(Z) \quad . \tag{4.4}$$

(Compare Fig. 12 with Fig. 8.) A_{LR} can thus serve as a probe of the virtual loop structure of the standard model, including as yet undetected particles coupled to the electroweak gauge bosons.[2,9,21] Furthermore, since $A_{LR}(Z)$ is largely independent of corrections other than oblique and initial weak vertices, it can be computed without a Monte Carlo. Another such quantity, affected only by oblique and weak vertex corrections, is the W vector boson mass M_W. The virtual corrections common to both impose a relationship between them, shown in Figure 13 for the standard model with unknown top and Higgs masses. Since the radiative corrections have *two* unknown parameters ($m_{\rm top}$ and $m_{\rm Higgs}$), one more experimental input [say, of the ρ-parameter, $\rho_*(0)$] is necessary to *test* the standard model including its radiative corrections. (This is a special case of a more general way of testing the SU(2)×U(1) electroweak gauge structure independently of the specific content of the oblique corrections.) Nevertheless, when combined with M_W, $A_{LR}(Z)$ can confine $m_{\rm top}$ and $m_{\rm Higgs}$ to some region of Figure 13. A_{LR} also places limits on proposed additions and modifications to the standard model, such as supersymmetry and technicolor. Table VI shows

the shifts in $A_{LR}(Z)$, as well as $A_{FB}(Z)$ and M_W, due to various kinds of exotic particles.[2]

Because of its unusual properties, A_{LR} can be measured with high precision at the SLC and LEP colliders, unlike A_{FB} (compare, Table I). For this reason, extra care should taken in its calculation. We have used BREM5 to compute the shifts in A_{LR} due to the weak box, initial/final and final QED corrections and added them to the results of EXPOSTAR. These predictions are displayed in Table VII for comparison to Table II of Lynn and Verzegnassi, which is based on the same corrections but has only one-photon radiation in the initial state. The results of Table VII constitute the most complete and accurate predictions for A_{LR} to date. There are two important limitations to the prediction of A_{LR}.[25] The largest is the photon self-energy (vacuum polarization) error (caused by the use of $e^+e^- \rightarrow$ *hadrons* collider data in dispersion relations), which could be reduced in the future through better measurement of the low-energy hadronic resonances. ($\delta A_{LR}^{vacpol}(Z) \simeq 0.0035$.) A smaller error arises from the imperfect cancellation of final-state strong interaction effects in $A_{LR}(Z)$, caused by the presence of a photon channel. ($\delta A_{LR}^{strong}(Z) \simeq 0.0005$.) The major experimental limitations are due to statistics (reducible with larger samples of events) and the uncertainty of the e^- beam polarization, which can be perhaps reduced to 1% by the use of a Compton polarimeter. ($\delta A_{LR}^{pol}(Z)/A_{LR}(Z) = \delta P/P$.) The experimental uncertainties are combined in Figure 14. With an e^- beam polarization of 45%, a polarization error of 1%, the current vacuum polarization data and 10^6 Z° events, $A_{LR}(Z)$ can be measured to an accuracy of ± 0.004. Together with the theoretical uncertainties, this fixes $s_*^2(Z)$ to ± 0.001. Figure 14 also compares the accuracy attainable with $A_{LR}^{hadrons}(Z)$ with that possible with $A_{FB}^{\mu^+\mu^-}(Z)$, very much to latter's disadvantage. Apart from poor statistics, A_{FB} is more sensitive to uncertainty in the beam energy, because it varies more rapidly with energy than does A_{LR}. The structure function approach to initial-state bremsstrahlung is ideally suited to incorporating the effect of an intrinsic beamspread, if this becomes necessary. In any case, intrinsic beamspread effects cancel out in A_{LR}.

5. Discussion and Conclusion

The basic set of electroweak observables presented here are sufficient to determine the gauge structure of the standard model. Using a subset of the relevant radiative corrections, the EXPOSTAR Monte Carlo is capable of computing to the necessary accuracy the following: the Z° cross sections to various types of final-state fermions, the forward-backward asymmetries and the left-right polarization asymmetry. The Z° peak cross sections and forward-backward asymmetry are not particularly sensitive to virtual corrections, but are strongly affected by initial-state bremsstrahlung. They can be adequately computed by simple Monte Carlo programs that include only initial-state radiation and arbitrarily adjustable electroweak parameters. The cross sections and A_{FB} are only able to test the standard model on a very general level that excludes the subtle effects of virtual corrections. The left-right polarization asymmetry, having certain unique properties, is capable of testing the standard model far more precisely and is highly sensitive to virtual corrections. Together with the W boson mass, it serves as a powerful check of electroweak loop physics. Such loop corrections must be included explicitly in any calculation of A_{LR}. On the other hand, we have seen that, at the Z° pole at least, radiation plays no important role in A_{LR}. There is also little need to take final-state effects into account in $A_{LR}(Z)$. Thus, the considerable work done already on the polarization asymmetry without radiation remains valid, and future work is freed from the need for the simulation of radiation and hadronization effects.[28]

As the SLC and LEP colliders move beyond the first stages of studying the electroweak neutral current, the polarization asymmetry will play a central role in precise tests of the standard model. With high statistics, A_{LR} becomes an indispensable tool for exploring the physics of virtual particles and probing for a new level of structure at mass scales inaccessible to present accelerators. The importance of A_{LR} in testing and reaching beyond the standard model underscores the crucial need for polarization at the SLC, LEP and e^+e^- colliders of the future.

Acknowledgements

We would like to thank the Mark II collaboration at SLAC for their support, encouragement and criticism. We are particularly indebted to James Alexander, Giovanni Bonvicini, Friedrich Dydak, Patricia Rankin, Luca Trentadue and B. F. L. Ward for many fruitful discussions.

Appendix: The Noodle Method

The Noodle method solves three major shortcomings of the standard Monte Carlo integration technique: finding a suitable approximant, inefficient sampling of the approximant space and slow event generation via inversion.

In the traditional Monte Carlo method, one computes $\int_S f$ by rewriting the integrand in terms of an approximate integrand g as $\int_{\tilde{S}} \frac{f}{g}$. The quantity $\frac{f}{g}$ is called the weight. In the Noodle method, g is defined automatically as follows: First, the region of integration S is decomposed into small sets over each of which the integrand f is roughly constant. Then for each set, the approximate integrand g is defined as exactly constant over the set and equal to f at least one point in the set. The graphs of S and $\tilde{S}$ resulting from this construction for the calculation of EXPOSTAR at $\sqrt{s} = 94$ GeV are shown in Figure 15a. By construction, g approximates f, and, since g is constant over each noodle, g can be integrated exactly. This solves the problem of finding a suitable approximate cross section.

We then generate values for the phase space variables with relative probability g. This is done by constructing an array called *noodle* via $noodle_i = noodle_{i-1} +$ the integral of g over the i^{th} set. Imagine a number of noodles all joined from end to end forming a long noodle. Thinking of $noodle_i$ as the sum of the lengths of the first i noodles, sampling uniformly along the length of the long noodle picks out a noodle with relative probability density g. Once a noodle is chosen, since g is constant within the set corresponding to the noodle, any point in the phase space within the set is equally likely to be chosen. Accordingly, we simply pick a random point within the set. It is fast because each generation of an event involves only a binary search algorithm for choosing a noodle and a random number generation. It is efficient in the sense that no point that is generated is rejected.

For this method to work better than the traditional Monte Carlo method, it is crucial to partition S into small sets so that f is indeed approximately constant

over each set. One way to achieve this is simply to cut up S at equal intervals so that, over S, $\frac{f}{g}$ takes values in a small interval around 1, say $(1-\epsilon, 1+\epsilon)$. Thus, if the graph of f has a tall but narrow spike at a point but is otherwise flat, the necessary number of noodles dictated by the width of the spike is clearly an overestimate for the rest of the region of integration.

In the spirit of replacing nontrivial analytical calculations by exact numerical calculations, it would be pleasing if there existed a numerical algorithm for finding an acceptable partition of S. The following algorithm is only a partial solution to this problem that presumes a knowledge of the general profile of the integrand: Start with an arbitrary partition of S. For each component of the partition, evaluate the function *wild*. If the component is *wild*, partition the component into smaller components until none of the components are *wild*. A component is *wild* if the integrand f fluctuates ***unacceptably*** inside the component. In EXPOSTAR, the region around the Z° pole and the region near the photon pole are defined to be *wild*.

The user has to define the *wild* function. Since the Noodle method automatically generates events, a list of events associated with unacceptable weights can readily be provided. This furnishes two pieces of information. It is an indication that the *wild* function is insufficiently defined. It also gives the user qualitative information about regions of the phase space over which the differential cross section has an unexpected structure. Once the *wild* function is adequately defined, the Noodle method generates a minimal partition of S that produces an extremely good weight distribution (Figures 15b, 15c and 16).

A complete description of the Noodle method along with a detailed example of application appears elsewhere.[20]

REFERENCES

1. A. Blondel, B. W. Lynn, F. M. Renard and C. Verzegnassi, Montpelier preprint PM/87–14 (1987).
2. B. W. Lynn, M. E. Peskin and R. G. Stuart, SLAC–PUB–3725 (1985); LEP *Yellow Book,* CERN 86–02, (1986), Vol. I, p. 90.
3. R. G. Stuart, D. Phil. Thesis, Oxford University (1985).
4. G. Passarino and M. Veltman, Nucl. Phys. **B160** (1979) 151.
5. F. A. Berends, G. J. H. Burgers and W. L. van Neerven, Phys. Lett. **B185** (1987) 395.
6. D. R. Yennie, S. C. Frautschi and H. Suura, Ann. Phys. (New York) **13** (1961) 379.
7. B. F. L. Ward, Int. Cen. Theo. Phys. preprint IC/86/211 (1986).
8. R. Kleiss, D. Phil. Thesis, University of Leiden (1982); F. A. Berends and R. Kleiss, Nucl. Phys. **B177** (1981) 237.
9. D. C. Kennedy and B. W. Lynn, SLAC–PUB–4039 (1988).
10. B. W. Lynn, G. Penso and C. Verzegnassi, Phys. Rev. **D35** (1987) 42.
11. B. W. Lynn, D. Phil. Thesis, Columbia University (1982).
12. S. Jadach, Max–Planck–Institut preprint MPI–PAE/PTh 6/87 (1987).
13. R. N. Cahn, Lawrence Berkeley preprint LBL–22601 (1986).
14. J. Alexander, G. Bonvicini, P. Drell and R. Frey, SLAC–PUB–4376.
15. O. Nicrosini and L. Trentadue, Phys. Lett. **B196** (1987) 551.
16. E. A. Kuraev and V. S. Fadin, Sov. J. Nucl. Phys. **41** (1985) 466.
17. G. Altarelli and G. Martinelli, LEP *Yellow Book,* CERN 86–02 (1986), Vol. I, p. 47.
18. L. Trentadue, private communication.

19. D. C. Kennedy, R. Kleiss, B. W. Lynn, R. G. Stuart and C. J. -C. Im (SLIKK), in preparation.

20. C. J. -C. Im, SLAC–PUB–4549.

21. B. W. Lynn and R. G. Stuart, Nucl. Phys. **B253** (1985) 216.

22. S. Jadach, J. H. Kuhn, R. G. Stuart and Z. Was, Max–Planck–Institut preprint MPI–PAE/PTh–71/87 (1987).

23. F. A. Berends, G. Burgers, W. Hollik and W. L. van Neerven, CERN preprint CERN–TH–4919/87 (1987).

24. W. Hollik, DESY preprint DESY 88–003.

25. B. W. Lynn and C. Verzegnassi, Phys. Rev. **D35** (1987) 3326.

26. M. Bohm and W. Hollik, Nucl. Phys. **B204** (1982) 45.

27. Kniehl, P. Krawczyk, J. H. Kühn and R. G. Stuart, Max–Planck–Institut preprint MPI–PAE/PTh 93/87. *All* initial-state QED effects, as shown in Ref. 16, can be written in the factorized form of Eq. 2.5: both "nonsinglet" (radiation and vertex corrections) and "singlet" (virtual and real pair production to all accessible pairs: electrons, muons, hadrons, etc.) terms. Convoluting once, the effects can be put into a form factor $H(\chi)$. The corrected $\widetilde{A}_{LR}$ is related to the uncorrected A_{LR} by:

$$\widetilde{A}_{LR}(s) = A_{LR}(s)\left\{1 + \frac{\int_0^1 d\chi H(\chi)\left[\frac{A_{LR}[(1-\chi)s]}{A_{LR}(s)} - 1\right]\sigma[(1-\chi)s]}{\int_0^1 d\chi H(\chi)\sigma[(1-\chi)s]}\right\} .$$

$A_{LR}(s)$ is not a steep function of s. (Without the photon channel, A_{LR} would be constant.) Furthermore, $H(\chi)$ is dominated by the infrared region, $\chi \to 0$. Hence, the second term in brackets is small, and the initial-state effects cancel almost completely.

28. In fact, a reasonable value of $A_{LR}(Z)$ can be obtained by using the simple-minded formula, Eq. 4.2, and replacing the s_θ^2 in the coupling with $s_*^2(Z)$.

(This neglects the photon channel and the initial weak corrections.) We get

$$A_{LR}(Z) \simeq \frac{2[1-4s_*^2(Z)]}{1+[1-4s_*^2(Z)]^2} \quad .$$

From Fig. 2b, we read off $s_*^2(z) = 0.2146$, so that $A_{LR}(z) = 0.278$, as compared to 0.271 in Table II, an error of 0.007.

29. SLC Polarization Group/SLAC Mark II Collaboration.

Table Captions

Note: All Monte Carlo runs on EXPOSTAR with 10^5 events.
Hadrons = 2 $u\bar{u}$ + 3 $d\bar{d}$. Total = Hadrons + 2 $\mu^+\mu^-$.

I. Effect of radiative corrections to various observables at the Z° peak.

II. Observables at the Z° peak with standard input.

III. Effect of cuts on the cross sections and forward-backward asymmetries at the Z° peak; with standard input.

IV. Effect of heavy virtual top and Higgs on observables at the Z° peak; with standard input.

V. Effect of cuts on left-right asymmetry at Z° peak; with standard input.

VI. Shifts to $A_{LR}^{\mu^+\mu^-}(Z)$, $A_{FB}^{\mu^+\mu^-}(Z)$, and M_W due to new physics; with standard input.[2]

VII. Predictions for A_{LR} from EXPOSTAR combined with shifts from BREM5 due to: weak boxes, initial/final and final QED; with standard input.

TABLE I

Effect of Radiative Corrections on Z Peak Cross Section

Example: $M_Z = 93$ GeV, $\Gamma_Z = 2.6$ GeV, $s_\theta^2 = 0.223$

	$\sigma^{\mu^+\mu^-}$(pb)[1]	Peak (GeV)[1]	$A_{\rm FB}^{\mu^+\mu^-}$[1]	$A_{\rm LR}^{\mu^+\mu^-}$
Tree level[2]	1720	93.05	0.034	0.212
Changes due to:				
Initial QED[2]	−450	+70 MeV	−0.018	≤ -0.002
Final QED	+20	none	negligible	≤ -0.002
I/F QED	negligible	negligible	negligible	negligible
Oblique[2]	−25	negligible	negligible	+0.014
Initial weak[2]	≤ -10	none	−0.001	−0.006
Final weak[2]	≤ -10	none	−0.001	negligible
Weak boxes	negligible	none	negligible	negligible
Uncertainties due to cuts and $\vec{p}_\perp$*:*				
Endcap	±0.4%	negligible	±0.001	negligible
Acollinearity	negligible	none	negligible	negligible
Realistic experimental goals:				
SLC/LEP	±3%	±50 MeV	±0.05	±0.004

1. Unpolarized.
2. Contained in EXPOSTAR. Other contributions obtained from BREM5 Monte Carlo. "Negligible" = "$\leq$ one part in 10^3."

TABLE II

Cross Sections and Asymmetries at Z°: Standard Input

Cross Sections (pb)

$\mu^+\mu^-$	$u\bar{u}$	$d\bar{d}$	*Hadrons*	*Total*
1360	4690	5970	27300	30010

Forward–Backward Asymmetries to $\mu^+\mu^-$

	$A_{FB}^{\mu^+\mu^-}$	$A_{FB}^{\mu^+\mu^-,pol}$
	0.039	0.203

Forward–Backward Asymmetries to Hadrons

	$A_{FB}^{u\bar{u}}$	$A_{FB}^{u\bar{u},pol}$	$A_{FB}^{d\bar{d}}$	$A_{FB}^{d\bar{d},pol}$
	0.139	0.538	0.192	0.708

Left–Right Asymmetries

$\mu^+\mu^-$	$u\bar{u}$	$d\bar{d}$	*Hadrons*	*Total*
0.269	0.269	0.272	0.271	0.271

TABLE III

Cross Section and A_{FB} to $\mu^+\mu^-$ at Z° with Cuts

ξ= Acollinearity, $\cos\theta$= Endcap Cosine

		$\sigma^{\mu^+\mu^-}(pb)$	$A_{FB}^{\mu^+\mu^-}$
$\xi = 180°$	$\cos\theta = 1.00$	1360	0.039
	$\cos\theta = 0.98$	1320	0.039
	$\cos\theta = 0.80$	987	0.034
$\xi = 2°$	$\cos\theta = 1.00$	1330	0.045

TABLE IV

Effect of Virtual Top and Higgs at Z°

All masses in GeV

		$\sigma^{\mu^+\mu^-}(pb)$	Z° *Width (GeV)*	
$m_H = 100$	$m_t = 30$	1120	2.95	
	$m_t = 60$	1360	2.76	
	$m_t = 300$	1360	2.88	
	$m_t = 500$	1370	3.09	
$m_t = 60$	$m_H = 10$	1360	2.78	
	$m_H = 100$	1360	2.76	
	$m_H = 1000$	1360	2.75	
		$A_{FB}^{\mu^+\mu^-}$	$A_{LR}^{\mu^+\mu^-}$	$A_{LR}^{hadrons}$
$m_H = 100$	$m_t = 30$	0.034	0.266	0.251
	$m_t = 60$	0.039	0.269	0.271
	$m_t = 300$	0.064	0.329	0.331
	$m_t = 500$	0.121	0.426	0.430
$m_t = 60$	$m_H = 10$	0.038	0.274	0.276
	$m_H = 100$	0.039	0.269	0.271
	$m_H = 1000$	0.032	0.260	0.261

TABLE V

Left–Right Asymmetries at Z° with Cuts

ξ= Acollinearity, $\cos\theta$= Endcap Cosine

		$A_{LR}^{\mu^+\mu^-}$	$A_{LR}^{hadrons}$
$\xi = 180^\circ$	$\cos\theta = 1.00$	0.269	0.271
	$\cos\theta = 0.98$	0.269	0.271
	$\cos\theta = 0.80$	0.269	0.272
$\xi = 2^\circ$	$\cos\theta = 1.00$	0.270	0.273

TABLE VI

Shifts to Various Asymmetries and M_W from New Physics

Results are generic

One-Loop Physics	$\delta A_{LR}^{\mu^+\mu^-}$	$\delta A_{FB}^{\mu^+\mu^-}$	δM_W (MeV)
Heavy quark pair			
a) Large splitting	0.02	0.01	300
b) Degenerate	−0.004	−0.002	−42
Heavy lepton pair			
a) Large splitting $m_\nu = 0$	0.012	0.006	300
b) Degenerate	−0.0013	−0.0006	−14
Heavy squark pair			
a) Large splitting	0.02	0.01	300
b) Degenerate	0	0	0
Heavy slepton pair			
a) Large splitting	0.012	0.006	300
b) Degenerate	0	0	0
Winos			
a) $m_{3/2} \ll 100$ GeV	0.005	0.0025	100
b) $m_{3/2} \gg 100$ GeV	<0.001	<0.001	<10
Technicolor			
$SU_8 \times SU_8$	−0.04	−0.018	−500
O_{16}	−0.07	−0.032	−500
Strong Interaction Uncertainty	±.004	±.002	±25 MeV

TABLE VII

Cross Sections and A_{LR} with Residual Corrections
from BREM5: Weak Boxes, Initial/Final and Final QED
With Standard Input

Cross Sections (pb)

$\sqrt{s}$ (GeV)	$\mu^+\mu^-$	$u\bar{u}$	$d\bar{d}$	*Hadrons*	*Total*
93	880	3040	3860	17660	19420
94	1360	4690	5970	27300	30010
95	1030	3560	4530	20700	22760

Left–Right Asymmetries

$\sqrt{s}$ (GeV)	$\mu^+\mu^-$	$u\bar{u}$	$d\bar{d}$	*Hadrons*	*Total*
93	0.255	0.242	0.253	0.249	0.249
94	0.269	0.268	0.272	0.271	0.271
95	0.280	0.287	0.283	0.285	0.285

Figure Captions

Note: All Monte Carlo runs on EXPOSTAR with 10^5 events. Hadrons = 2 $u\bar{u}$ + 3 $d\bar{d}$. Total = Hadrons + 2 $\mu^+\mu^-$.

1. (a) Oblique corrections, (b) Vertex corrections, (c) Box corrections, (d) Absolute square of bremsstrahlung amplitude.

2. Running starred functions with oblique corrections as functions of timelike energy; with standard input:[9] (a) $4\pi/e_*^2$, (b) s_*^2, (c) $G_{\mu *}$, (d) ρ_*.

3. Z° resonance line shape, from 90 to 96 GeV, for muons. Parameters (by hand): $M_Z = 93$ GeV, ${s_\theta}^2 = 0.223$, $\Gamma_Z = 2.5$ GeV. Peak cross section: 1370 pb; peak position: 93.11 GeV. For comparison, see Ref. 5. Dashed: tree level; solid: EXPOSTAR. (a) Z° peak from 90 to 96 GeV: large dots show peak position and intersection of tree and radiation cross sections, respectively; (b) blow-up of peak region.

4. Left-right asymmetry $A_{\rm LR}$ from 90 to 100 GeV for muons. Parameters (by hand): $M_Z = 93$ GeV, ${s_\theta}^2 = 0.222$, $\Gamma_Z = 2.8$ GeV. For comparison, see Ref. 13.

5. Comparison of forward-backward and left-right asymmetries for muons using EXPOSTAR (solid), BREM5 (dashed), Lynn and Stuart[21] (dotted). With $M_Z = 94$ GeV, $m_{\rm top} = 60$ GeV, and $m_{\rm Higgs} = 100$ GeV. (a) Forward-backward asymmetry; (b) left-right asymmetry.

6. Muon (dotted), hadron (dashed) and total (dot-dashed) cross sections at the Z° peak, with standard input. (a) From 92 to 96 GeV. (b) Blow-up of peak area, showing only the muon and total cross sections.

7. Muon cross section at Z° peak showing effect of endcap cuts. Endcap cosine = 1.00 (dotted), 0.98 (dot-dashed) and 0.80 (dashed); with standard input.

8. $s_*^2(Z)$ as function of top (solid) and Higgs (dashed) masses; with standard input.[9]

9. Forward-backward (dotted) and polarized forward-backward (dot-dashed) asymmetries for muons; with standard input.

10. Left-right polarization asymmetry for various species: muons (dotted), up quarks (dashed), down quarks (long dashes), hadrons (solid) and total (dot-dashed); with standard input.

11. Forward-backward asymmetry for muons with endcap cuts. Endcap cosine = 1.00 (dotted), 0.98 (dot-dashes), and 0.80 (dashed). Left-right asymmetry for muons (solid); with standard input.

12. Left-right asymmetry at Z° versus top (solid) and Higgs (dashed) masses; with standard input.

13. $A_{\rm LR}(Z)$ versus M_W, with lines of constant top (dashed) mass and constant Higgs (solid) mass. (a) Top mass from 60 to 500 GeV. (b) Blow-up of lower left-hand corner of (a); with standard input.

14. Accuracy of experimental measurement of $A_{\rm LR}(Z)$ and $s^2_*(Z)$.[29]

15. Monte Carlo sampling space of EXPOSTAR divided into "noodles." (a) 94 GeV; (b) 110 GeV; (c) 210 GeV center-of-mass energy. $P_\pm$'s are integrated radiation distributions (integrals of approximant D's; see Eq. 2.5 in text). Large bulge (not to scale) is Z° peak. Bulge at far corner is photon peak. Note narrowing of Z° peak with increasing energy; with standard input.[20]

16. A typical weight distribution for the EXPOSTAR Monte Carlo; with standard input, at 110 GeV center-of-mass energy.[20]

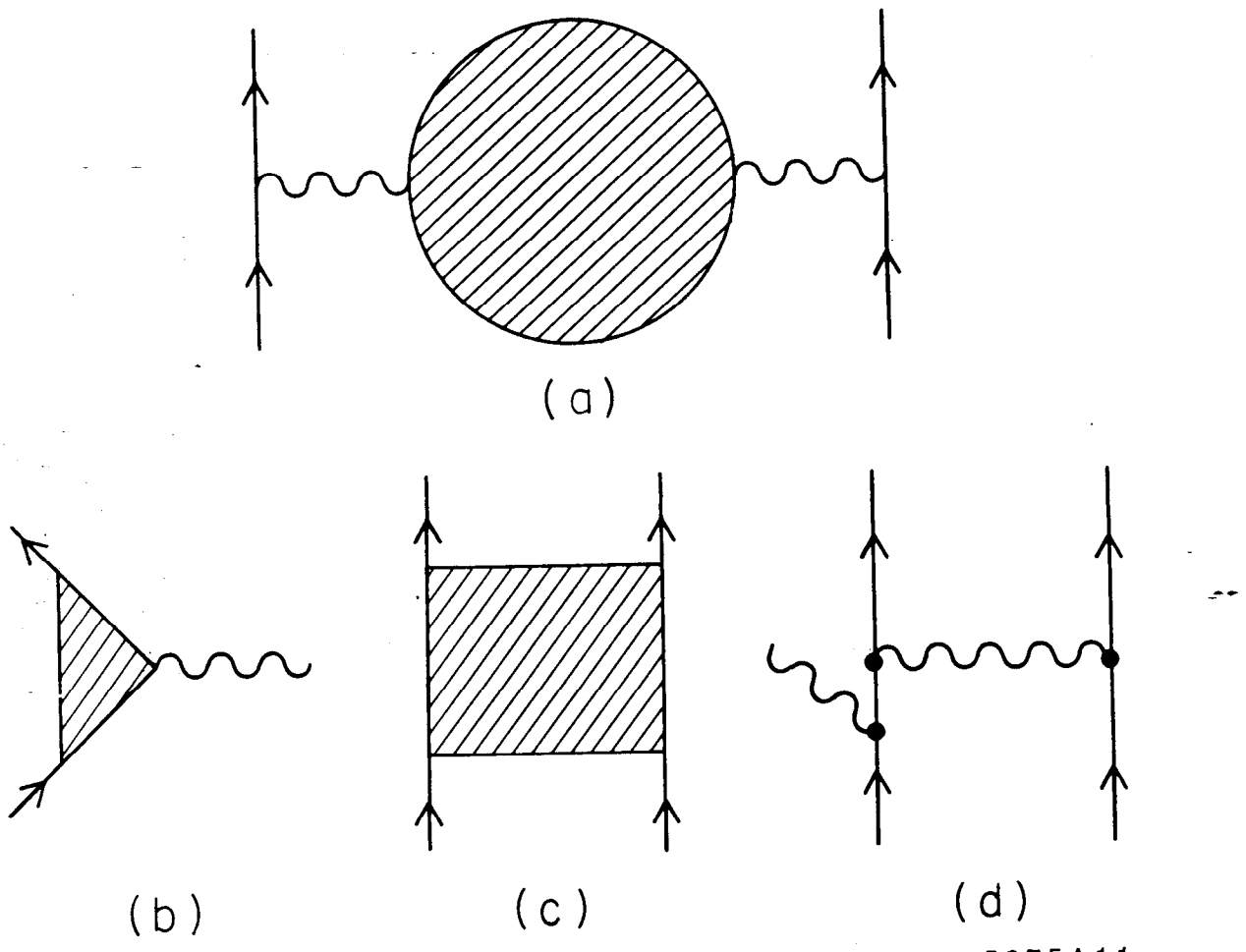

Fig. 1

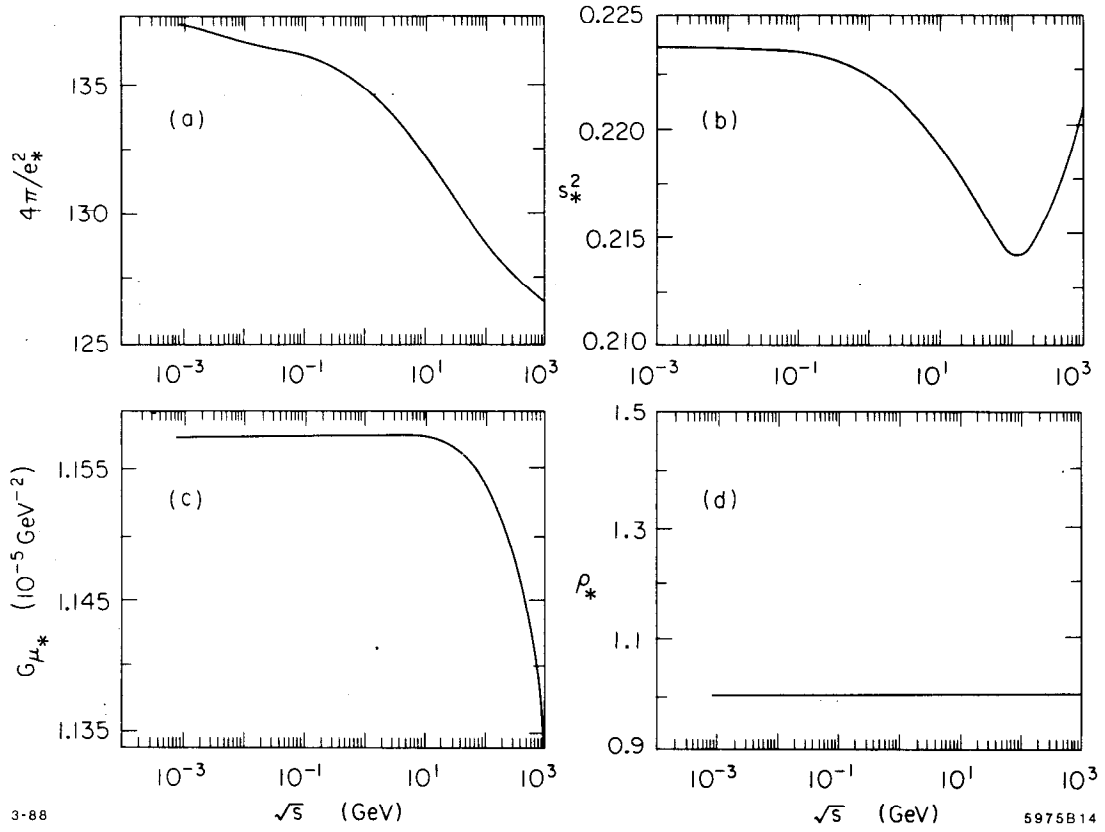
(a)
(b)
(c)
(d)
$4\pi/e_*^2$
135
130
125
s_*^2
0.225
0.220
0.215
0.210
G_{μ_*} $(10^{-5}\,GeV^{-2})$
1.155
1.145
1.135
ρ_*
1.5
1.3
1.1
0.9
10^{-3}
10^{-1}
10^{1}
10^{3}
$\sqrt{s}$ (GeV)
3-88
5975B14

Fig. 2

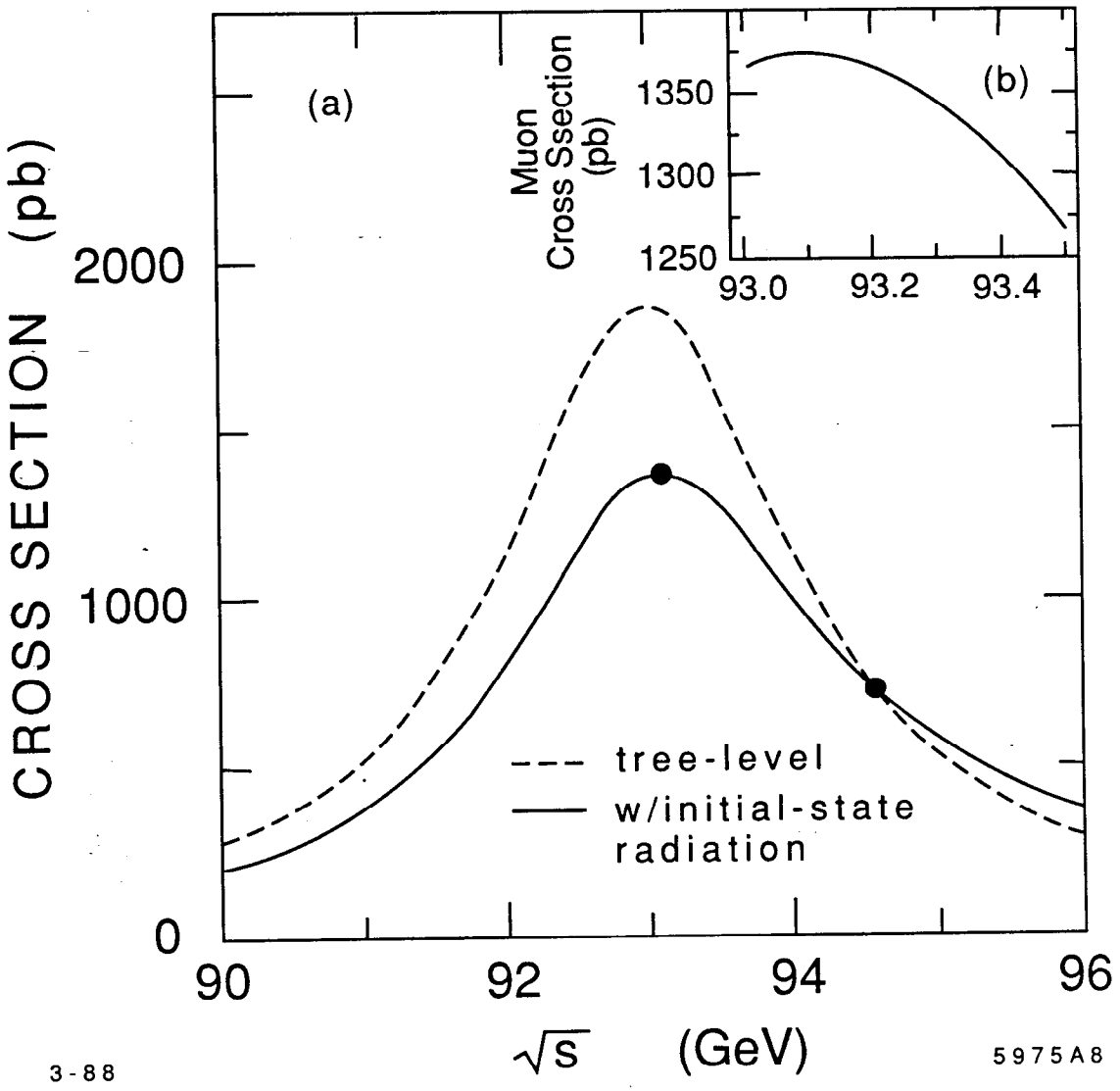
(a)
(b)
Muon
Cross Ssection
(pb)
1350
1300
1250
93.0
93.2
93.4
CROSS SECTION (pb)
2000
1000
0
90
92
94
96
tree-level
w/initial-state
radiation
√s (GeV)
3-88
5975A8

Fig. 3

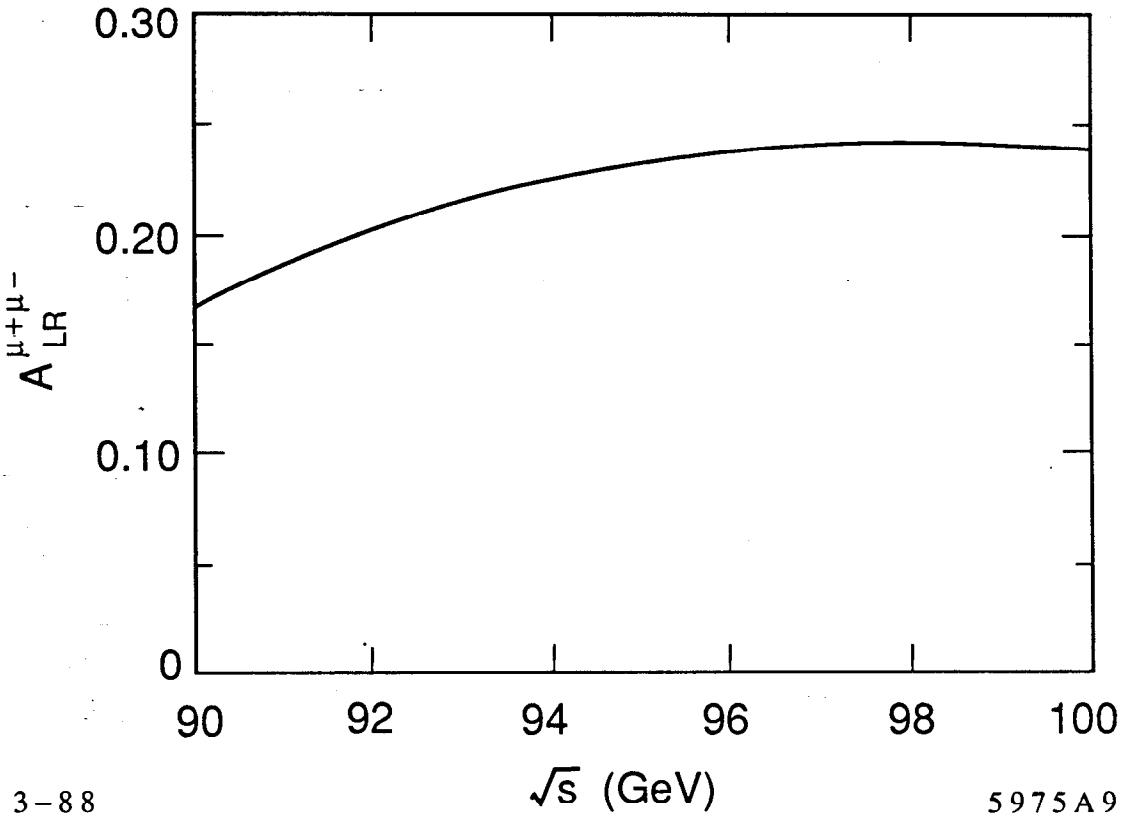

Fig. 4

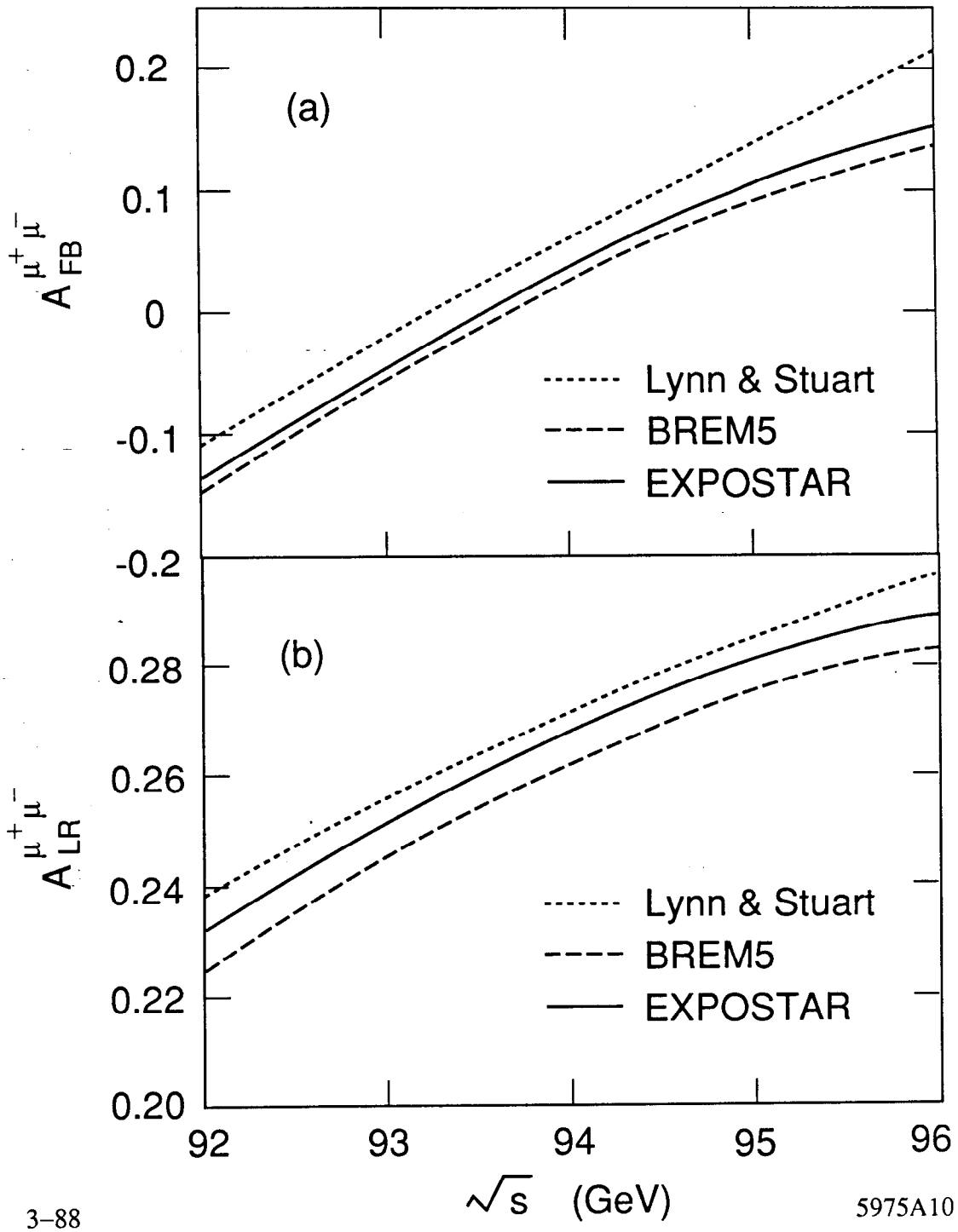
(a)
$A_{FB}^{\mu^+\mu^-}$
0.2
0.1
0
-0.1
-0.2
Lynn & Stuart
BREM5
EXPOSTAR
(b)
$A_{LR}^{\mu^+\mu^-}$
0.28
0.26
0.24
0.22
0.20
Lynn & Stuart
BREM5
EXPOSTAR
92
93
94
95
96
$\sqrt{s}$ (GeV)
5975A10

Fig. 5

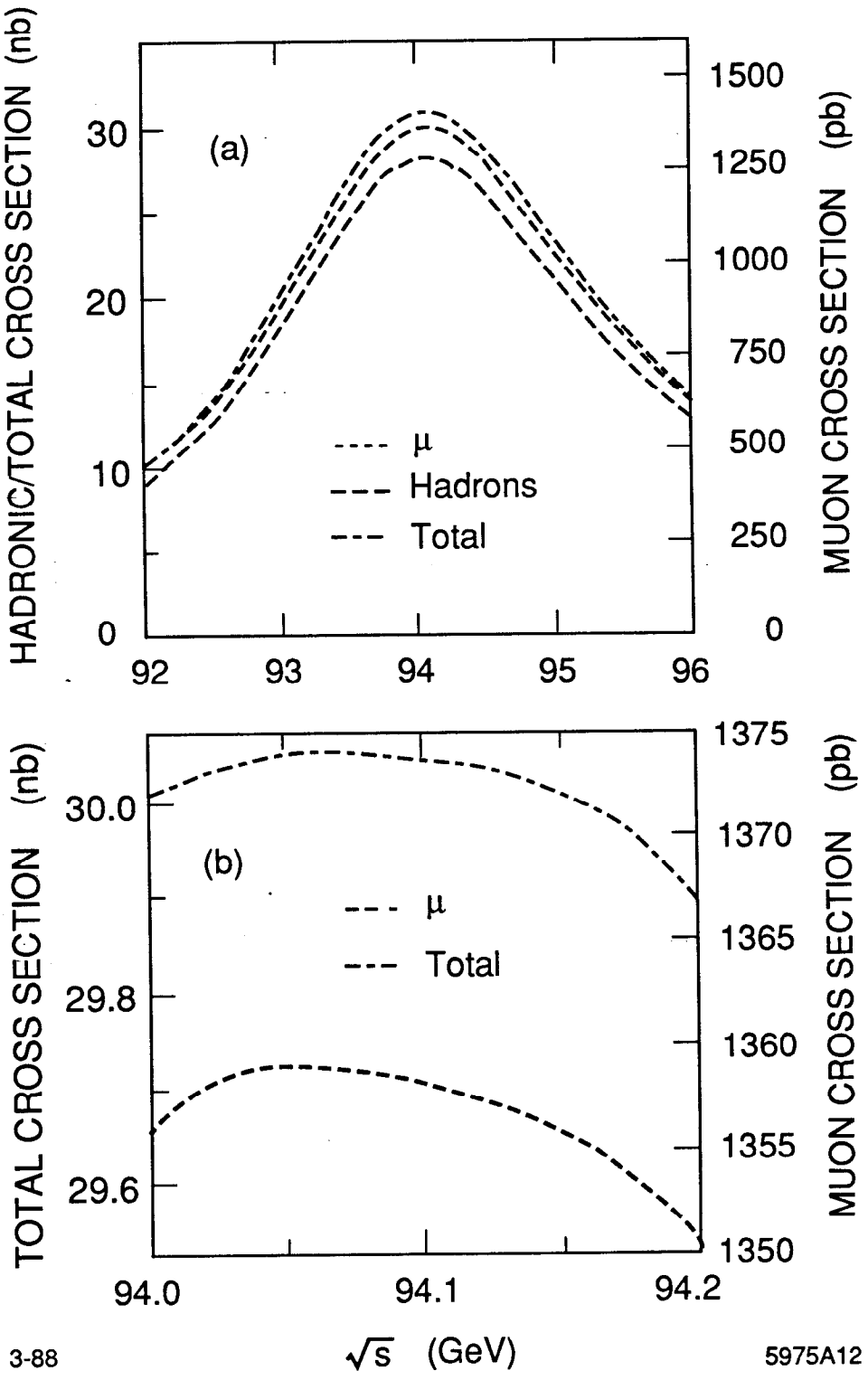
HADRONIC/TOTAL CROSS SECTION (nb)
MUON CROSS SECTION (pb)
(a)
μ
Hadrons
Total
30
20
10
0
1500
1250
1000
750
500
250
0
92
93
94
95
96
TOTAL CROSS SECTION (nb)
MUON CROSS SECTION (pb)
(b)
μ
Total
30.0
29.8
29.6
1375
1370
1365
1360
1355
1350
94.0
94.1
94.2
√s (GeV)
3-88
5975A12

Fig. 6

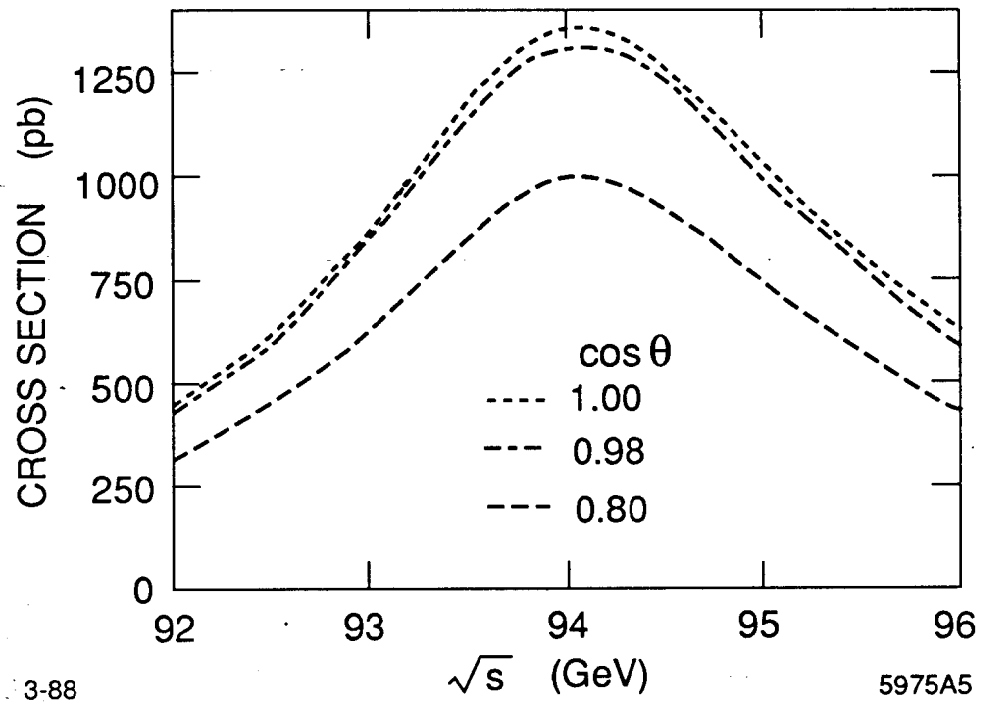
CROSS SECTION (pb)
1250
1000
750
500
250
0
92
93
94
95
96
√s (GeV)
cos θ
---- 1.00
--- 0.98
--- 0.80
3-88
5975A5

Fig. 7

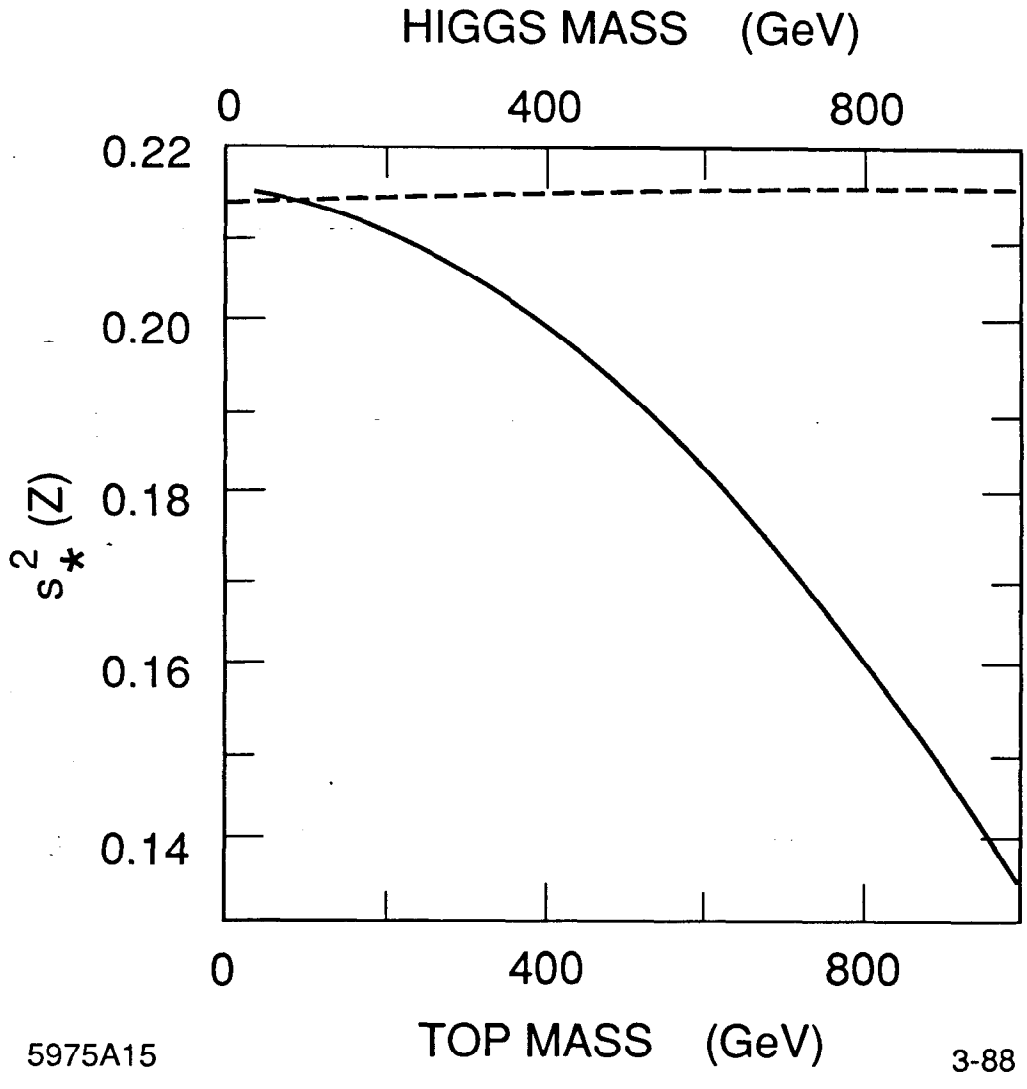
HIGGS MASS (GeV)
0
400
800
0.22
0.20
0.18
0.16
0.14
$s^2(Z)$*
0
400
800
TOP MASS (GeV)
5975A15
3-88

Fig. 8

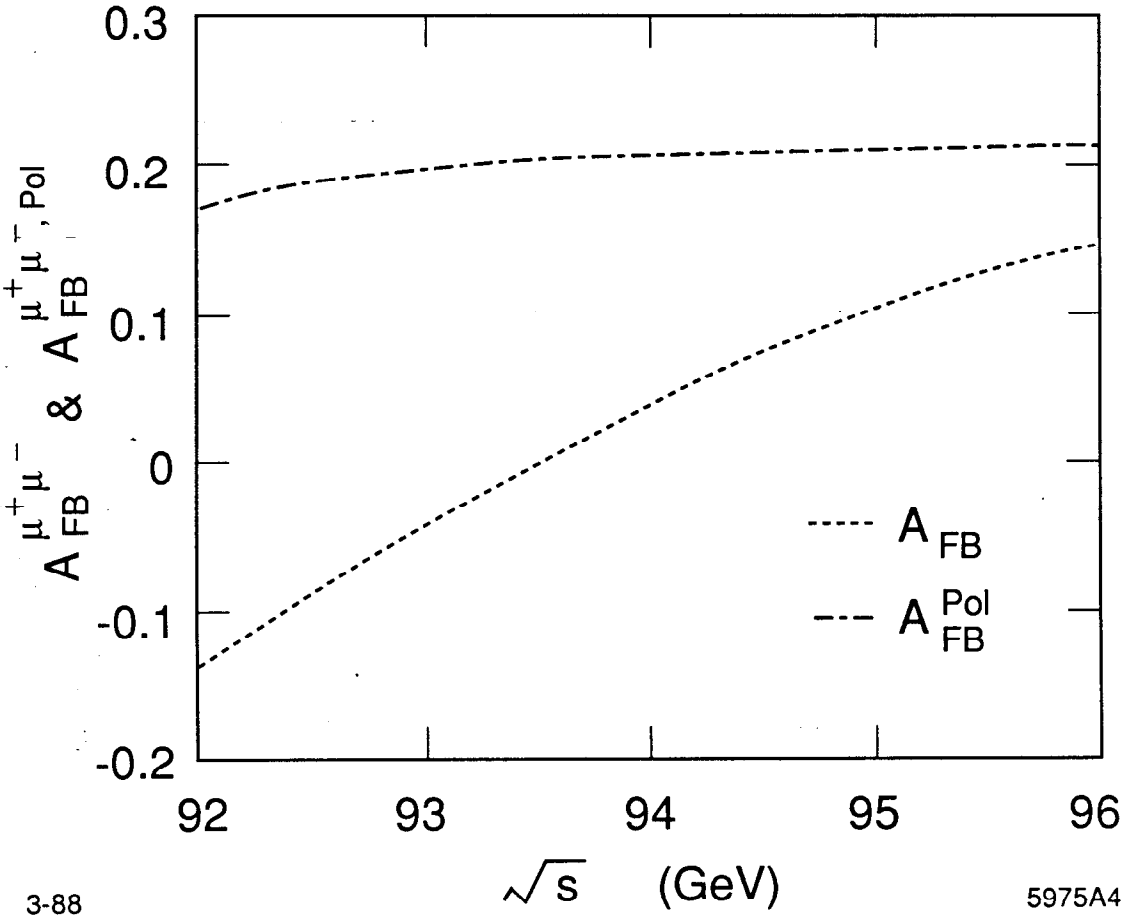
0.3
0.2
0.1
0
-0.1
-0.2
92
93
94
95
96
$A_{FB}^{\mu^+\mu^-}$ & $A_{FB}^{\mu^+\mu^-,Pol}$
$\sqrt{s}$ (GeV)
A_{FB}
A_{FB}^{Pol}
3-88
5975A4

Fig. 9

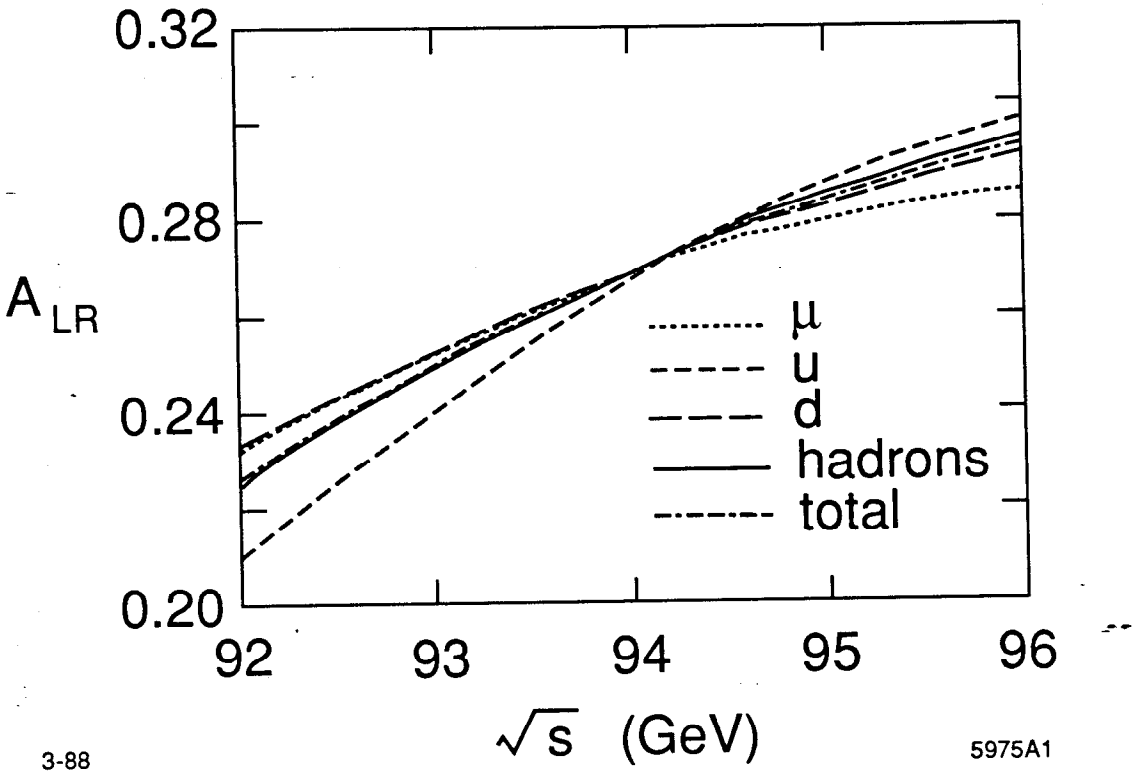
0.32
0.28
0.24
0.20
A_{LR}
92
93
94
95
96
$\sqrt{s}$ (GeV)
μ
u
d
hadrons
total
3-88
5975A1

Fig. 10

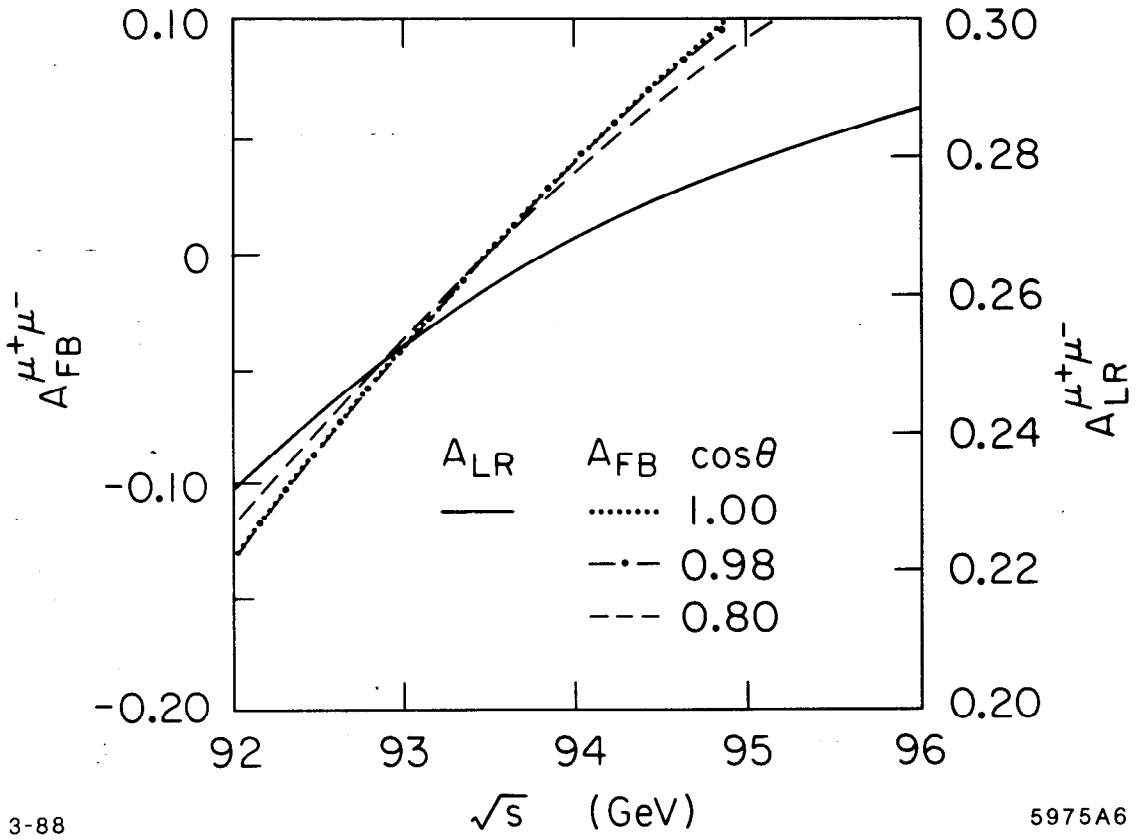
0.10
0
-0.10
-0.20
0.30
0.28
0.26
0.24
0.22
0.20
92
93
94
95
96
$A_{FB}^{\mu^+\mu^-}$
$A_{LR}^{\mu^+\mu^-}$
$\sqrt{s}$ (GeV)
A_{LR}
A_{FB} cosθ
1.00
0.98
0.80
3-88
5975A6

Fig. 11

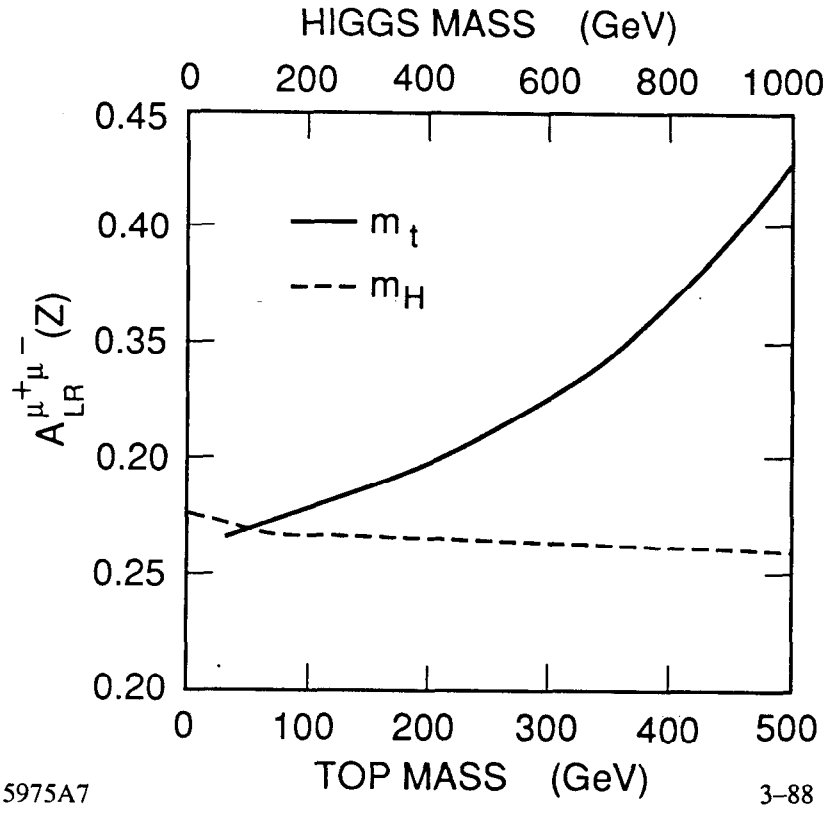
HIGGS MASS (GeV)
0
200
400
600
800
1000
0.45
0.40
0.35
0.20
0.25
0.20
m_t
m_H
$A_{LR}^{\mu^+\mu^-}(Z)$
0
100
200
300
400
500
TOP MASS (GeV)
5975A7
3–88

Fig. 12

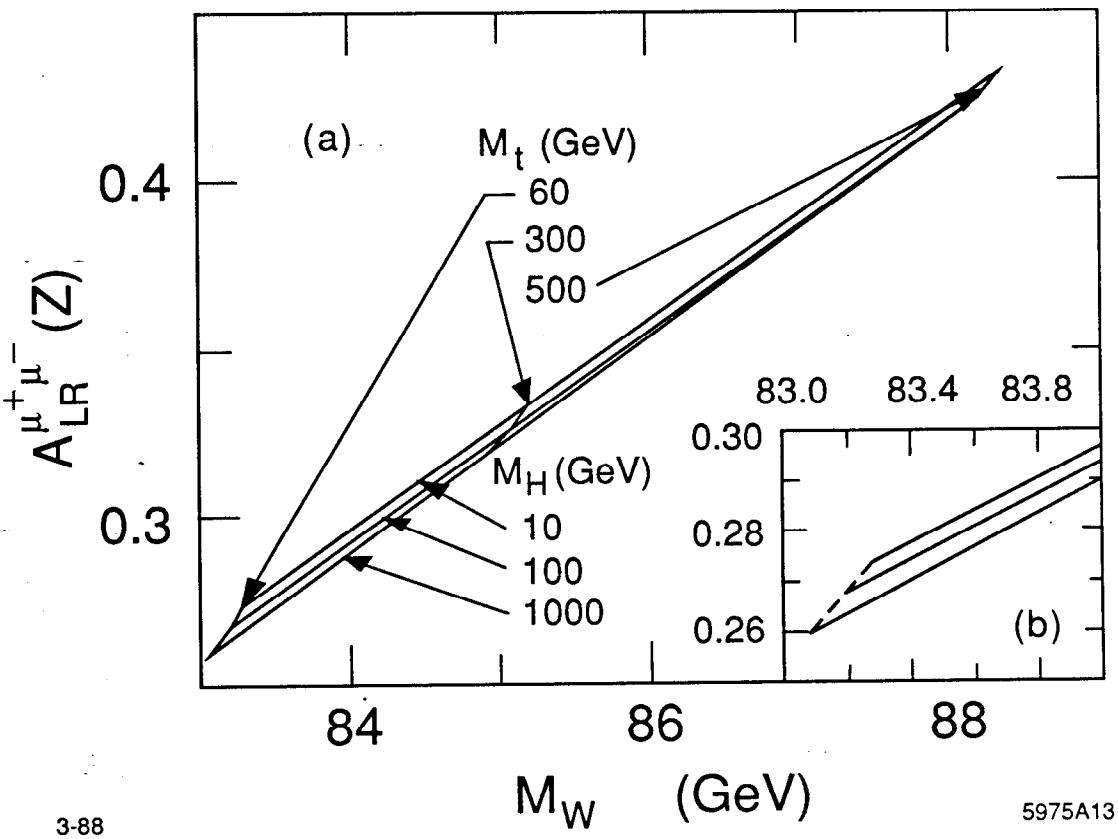
(a)
M_t (GeV)
60
300
500
M_H (GeV)
10
100
1000
0.4
0.3
$A_{LR}^{\mu^+\mu^-}(Z)$
84
86
88
M_W (GeV)
83.0
83.4
83.8
0.30
0.28
0.26
(b)
3-88
5975A13

Fig. 13

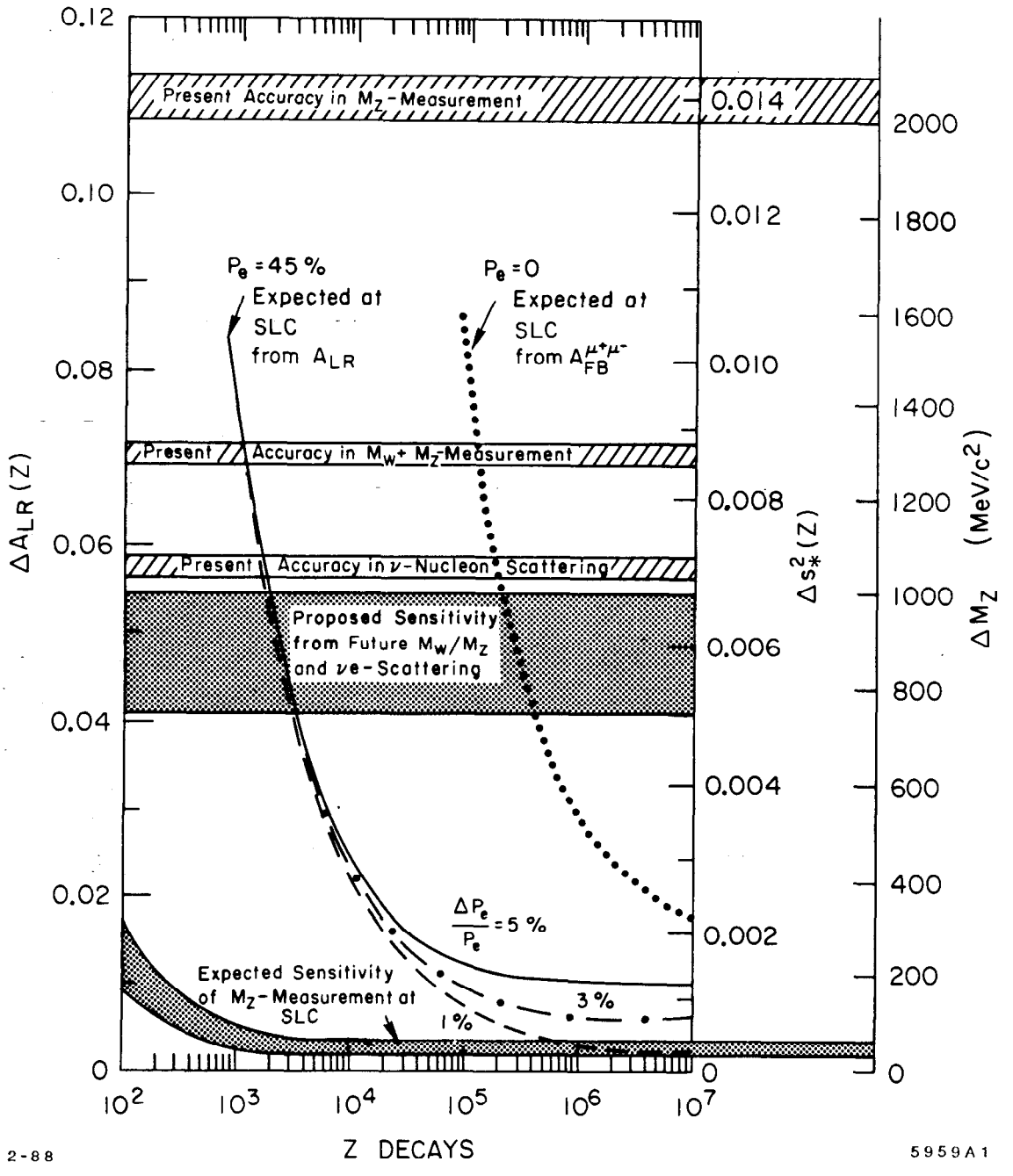
0.12
0.10
0.08
0.06
0.04
0.02
0
$\Delta A_{LR}(Z)$
Present Accuracy in M_Z-Measurement
0.014
0.012
0.010
0.008
0.006
0.004
0.002
0
$\Delta s^2_*(Z)$
2000
1800
1600
1400
1200
1000
800
600
400
200
0
ΔM_Z (MeV/c^2)
P_e = 45 % Expected at SLC from A_{LR}
P_e = 0 Expected at SLC from $A_{FB}^{\mu^+\mu^-}$
Present Accuracy in M_W+ M_Z-Measurement
Present Accuracy in ν-Nucleon Scattering
Proposed Sensitivity from Future M_W/M_Z and νe-Scattering
$\frac{\Delta P_e}{P_e}$ = 5 %
3 %
1 %
Expected Sensitivity of M_Z-Measurement at SLC
10^2
10^3
10^4
10^5
10^6
10^7
Z DECAYS
2-88
5959A1

Fig. 14

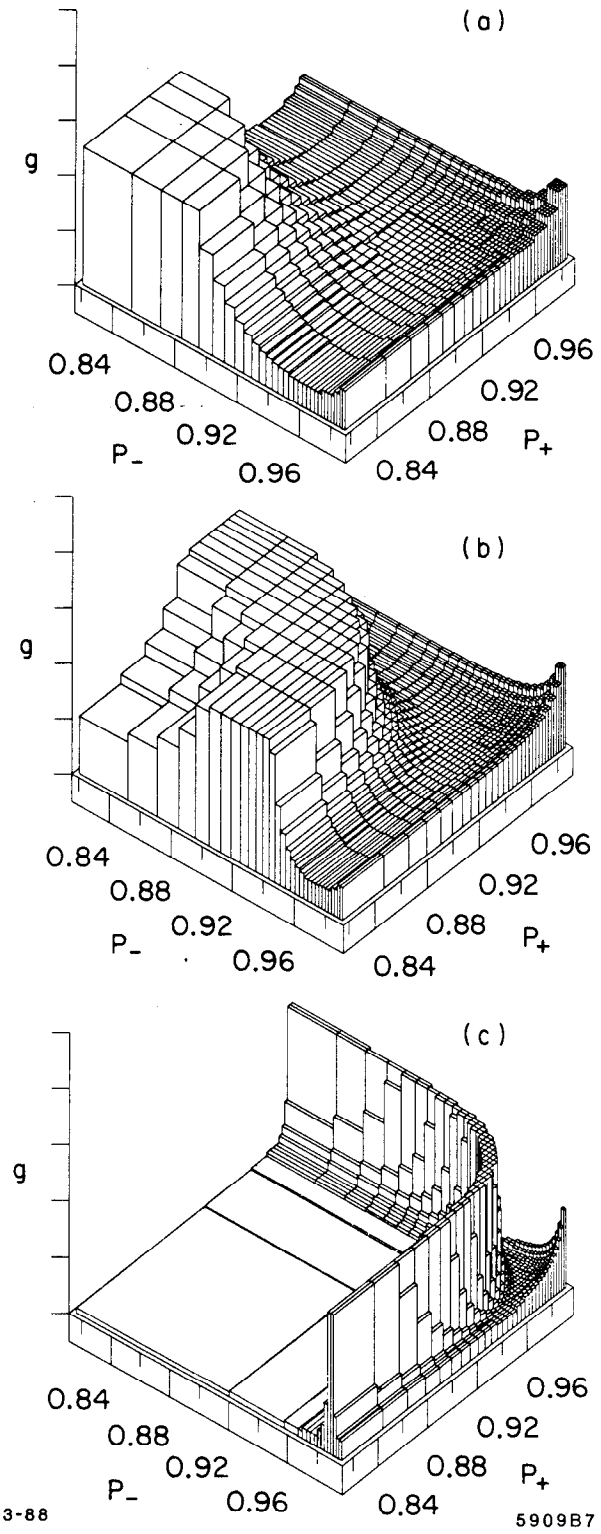
(a)
g
0.84
0.88
0.92
0.96
P-
0.84
0.88
0.92
0.96
P+
(b)
g
0.84
0.88
0.92
0.96
P-
0.84
0.88
0.92
0.96
P+
(c)
g
0.84
0.88
0.92
0.96
P-
0.84
0.88
0.92
0.96
P+
3-88
5909B7

Fig. 15

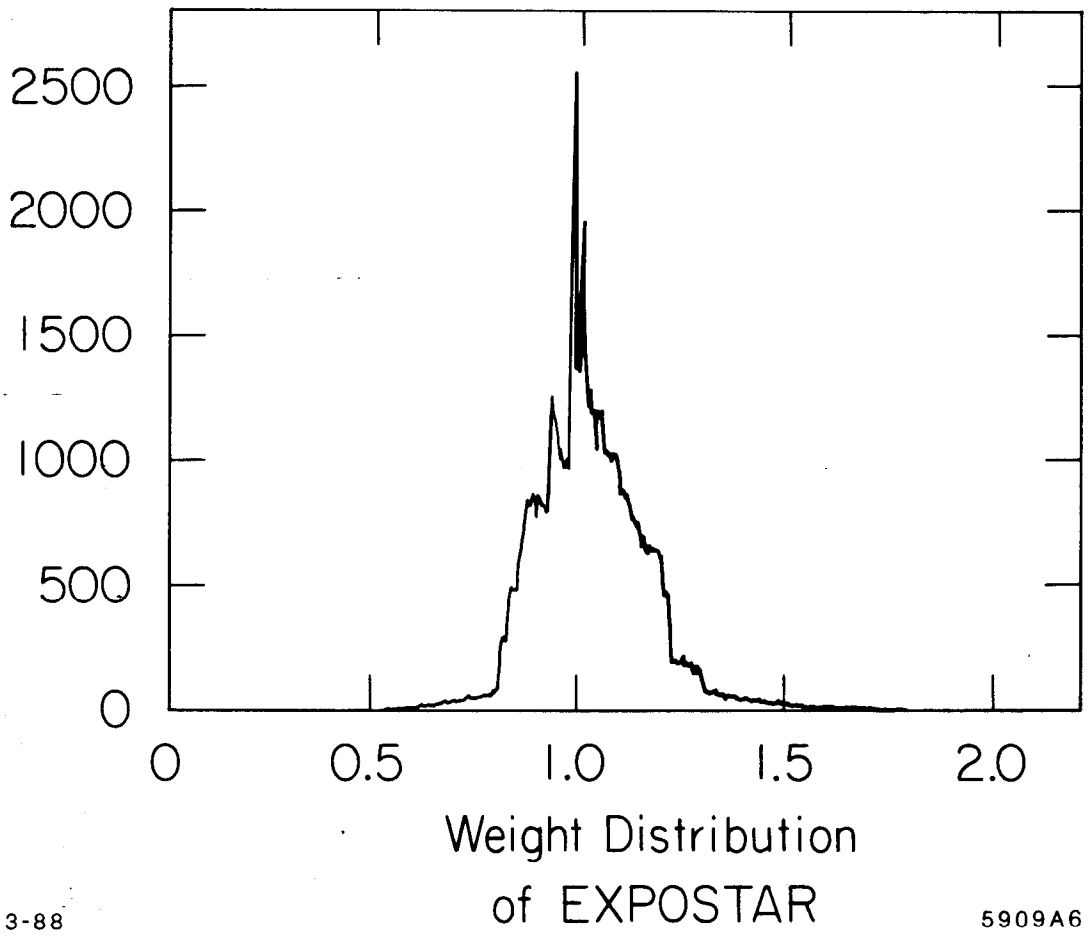
2500
2000
1500
1000
500
0
0
0.5
1.0
1.5
2.0
Weight Distribution
of EXPOSTAR
3-88
5909A6

Fig. 16